Distinct Mechanoresponsive Luminescence, Thermochromism, Vapochromism, and Chlorine Gas Sensing by a Solid-State Organic Emitter

Anirban Adak,[†,∇] Tamas Panda,[‡,∇] Anju Raveendran,[§] Kochan Sathyaseelan Bejoymohandas,[§] K. S. Asha,[∥] A. P. Prakasham,[⊥] Balaram Mukhopadhyay,*[,†] and Manas K. Panda*[,§,#]

[†]Department of Chemical Science, Indian Institute for Science and Educational Research Kolkata, Mohanpur 741246, Kolkata, India

[‡]New York University Abu Dhabi, Saadiyat Island, Abu Dhabi, United Arab Emirates, P.O. Box 129188

[§]Photosciences & Photonics Section, Chemical Science & Technology Division, CSIR-National Institute for Interdisciplinary Science & Technology, Thiruvanthapuram 695019, Kerala, India

[∥]School of Chemistry, Indian Institute for Science and Educational Research, Thiruvanthapuram 695551, Kerala, India

[⊥]Department of Chemistry, Indian Institute of Technology Bombay, Mumbai 400076, India

[#]Academy of Scientific and Innovative Research (AcSIR), New Delhi 110025, India

S *Supporting Information*

ABSTRACT: In this study, we report a synthetically simple donor−acceptor (D−A)-type organic solid-state emitter **1** that displays unique fluorescence switching under mechanical stimuli. Orange and yellow emissive crystals of **1** (**1O**, **1Y**) exhibit an unusual "back and forth" fluorescence response to mechanical force. Gentle crushing (mild pressure) of the orange or yellow emissive crystal results in hypsochromic shift to cyan emissive fragments (λ_{em} = 498−501 nm) with a large wavelength shift $\Delta\lambda_{em}$ = −71 to −96 nm, while further grinding results in bathochromic swing to green emissive powder λ_{em} = 540−550 nm, $\Delta\lambda_{em}$ = +40 to 58 nm. Single-crystal X-ray diffraction study reveals that molecules are packed by weak interactions, such as C−H⋯π, C−H⋯N, and C−H⋯F, which facilitate intermolecular charge transfer in the crystal. With the aid of structural, spectroscopic, and morphological studies, we established the interplay between intermolecular and intramolecular charge-transfer interaction that is responsible for this elusive mechanochromic luminescence. Moreover, we have also demonstrated the application of this organic material for chlorine gas sensing in solid state.
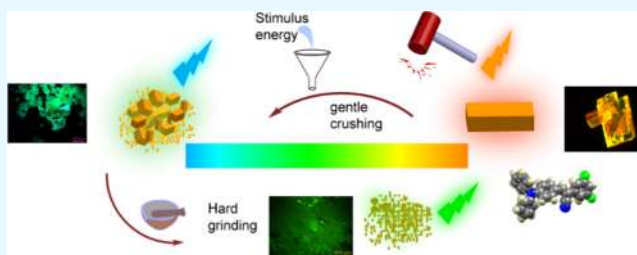
INTRODUCTION

In recent years, solid-state photoluminescent (PL) materials have attracted considerable research interest due to their wide range of applications in optoelectronics,[1−6] memory devices,[7,8] solid-state lasers,[8−11] security markers,[12−15] and bio-markers.[16−18] Specifically, the emitters that can switch their luminescence in response to external stimuli, such as heat, moisture, mechanical pressure, solvent vapor, or any specific gas, are of special interest for developing smart sensors and switches.[19−31] Mechanochromic luminescence (MCL) is a phenomenon where the change in photoluminescence is triggered by anisotropic or isotropic mechanical stress. A number of organic or inorganic materials that display MCL behavior have been reported so far.[32−37] To mention a few, Ito and co-workers reported a number of gold−isocyanide complexes that exhibited mechanochromic luminescence upon grinding.[38−40] Park and co-workers reported several cyano-styryl-based derivatives, which showed multistimuli-responsive luminescence in the solid state.[41,42] Recently, Weder and co-workers have reported several polymeric systems
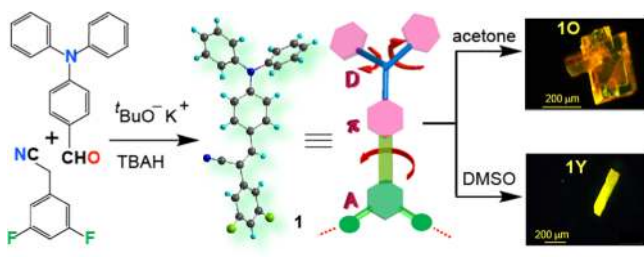
that displayed unique mechanochromic luminescence behavior.[43−46] Although materials that exhibit bathochromic luminescence shift upon mechanical grinding are very common, the examples of hypsochromic shift are rather limited.[47−51] Herein, we report a synthetically simple charge-transfer material ((*Z*)-2-(3,5-difluorophenyl)-3-(4-(diphenylamino)phenyl)-acrylonitrile, molecular compound is denoted as **1**, Scheme 1) composed of diphenylamine (DPA) donor and −F and −CN groups as acceptor that displays a unique multistage mechanochromic luminescence. Upon application of mechanical pressure, crystal forms of **1** show initial hypsochromic PL shift, followed by bathochromic PL shift. To the best of our knowledge, this is the first example of purely organic material that shows such "back and forth" wavelength switching under mechanical stimuli. In addition to mechanofluorochromism, the same material also exhibits thermo-/vapochromic fluorescence.

Scheme 1. Synthetic Scheme of 1 and Crystallization Route for 1O and 1Y

Figure 1. (a) Solution-state UV−vis, fluorescence, and excitation spectra of **1** (CHCl$_3$ 1 × 10^{-5} M solution); (b) DFT-calculated HOMO and LUMO orbitals of **1**; (c) UV−vis, fluorescence, and excitation spectra of **1** drop-cast thin film (from CHCl$_3$ 1 × 10^{-3} M solution); and (d) solid-state absorption spectra of small crystals of **1Y** and **1O**.

With the aid of detailed spectroscopic and structural study, we demonstrate here the interplay between intermolecular charge-transfer interaction and intramolecular charge-transfer (ICT) interaction during the course of mechanochromic fluorescence switching. Moreover, we have demonstrated the application of this material in gas sensing. Both crystal and ground powder are capable of detecting chlorine gas (evolved from commercial bleaching powder upon addition of small amount of water) by changing its fluorescence intensity. Although there are few examples of inorganic- and composite-based solid-state chlorine gas sensors,[52−55] reports of purely organic-based chlorine gas sensors are rare. According to our literature study, porphyrin-based film is the only example of organic material that showed chlorine gas-sensing property.[56]

Compared to this report, our solid-state approach is much simpler, easy to synthesize the compound in pure form, and thus cost-effective. More importantly, it is a single molecular component material that exhibits tunable solid-state emission, multistimuli responsivity, and gas-sensing property. Such material could have potential application in smart optoelectronics and sensing devices.

■ RESULTS AND DISCUSSION

Compound **1** was synthesized by one-step Knoevenagel condensation reaction between 4-(diphenylamino)-benzaldehyde and 3,5-difluorobenzyl cyanide in 80% yield (Scheme 1). Recrystallization of **1** from different solvents produced distinctly fluorescent forms. Yellow emissive crystals (**1Y**) were obtained from dimethyl sulfoxide solution, whereas orange emissive crystals (**1O**) were obtained from acetone solution (Scheme 1).

As-obtained product **1** was characterized by ^{1}H NMR spectroscopy, ^{13}C NMR spectroscopy, and high-resolution mass spectrometry (HRMS) (Figures S1−S3, Supporting Information (SI)). Thermogravimetric analysis (TGA) and differential scanning calorimetry (DSC, Figures S4 and S5, SI) showed that the crystals are stable up to 200 °C and have melting point in the range of 125−127 °C. UV−vis spectra of **1** (in CHCl$_3$, 1 × 10^{-5} M) showed two absorption bands, one at λ_{max} = 298 nm and a broad band in the 340−490 nm range with λ_{max} = 410 nm (Figure 1a). Comparing the absorption band of the individual components and the product, the 410 nm band can be assigned as intramolecular charge-transfer (ICT) absorption involving the interaction between donor diphenyl-amine group and acceptor −CN/−F group of **1**. Density functional theory (DFT) calculation reveals that the highest occupied molecular orbital (HOMO) is located on donor diphenylamine group, whereas lowest unoccupied molecular orbital (LUMO) is centered on −CN/−F acceptor, in line with the above observation (Figure 1b). Fluorescence spectra (in
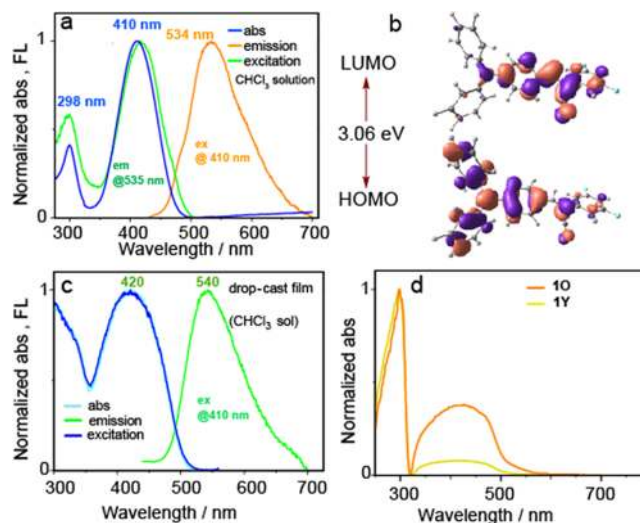
CHCl$_3$, 1 × 10^{-5} M, λ_{ex} = 410 nm) exhibited a broad green emissive band starting from 450 to 700 nm with $\lambda_{em,max}$ = 534 nm with a Stokes shift of 5663 cm^{-1} (Figure 1a). This band is attributed to intramolecular charge-transfer (ICT, ^{1}CT → S$_0$ transition) fluorescence. As expected for ICT compound, solvatochromic fluorescence shift was observed for **1** (Figure S6, SI).[57,58] Indeed, our DFT calculation reveals smaller HOMO−LUMO gap in polar solvent compared to nonpolar solvent (Figure S7, SI), supporting the above observation.

Next, we have carried out solid-state spectra of **1** drop-cast thin film and in crystalline state. Compared to the solution spectra, the charge-transfer band in drop-cast film (CHCl$_3$ solution, 1 × 10^{-3} M, Figure 1c) slightly red-shifted (∼10 nm) and became broader, suggesting the decrease in the HOMO−LUMO gap in film state. Fluorescence spectra of the thin film displayed a green emission band at 540 nm, which is assigned for ICT, ^{1}CT → S$_0$ transition. Similar to thin film, the UV−vis spectra of the crystals of **1Y**, **1O** exhibit a broad charge-transfer band in the range of 322−550 nm (Figure 1d).

Solid-state fluorescence spectra of pristine **1Y** crystal displays an emission band at $\lambda_{em,max}$ = 572 nm, whereas pristine **1O** crystal shows emission band at 595 nm (Figure 2c,d, yellow and orange lines, respectively). Quantum yields (QYs) of the crystals are much higher compared to those in solution of **1**, indicating the crystallization-induced emission enhancement behavior of this compound. As listed in Table S1, the absolute quantum yields of **1Y** and **1O** crystals are 0.34 and 0.30, respectively, but 0.017 in chloroform solution (with reference to fluorescein dye). This could be credited to intermolecular interactions in densely packed media that prevent nonradiative loss of excited energy and increase the quantum yield in solid state. The red-shifted luminescence of **1Y** and **1O** crystals (compared to solution) is expected to be contributed from an excited state governed by intermolecular interactions. Accordingly, fluorescence excitation spectra of both the crystals, **1Y** and **1O** (by monitoring the emission at 572 and 595 nm, respectively), exhibit a band at 515 nm (**1Y**) and 529 nm (**1O**), which can be attributed to intermolecular charge-transfer
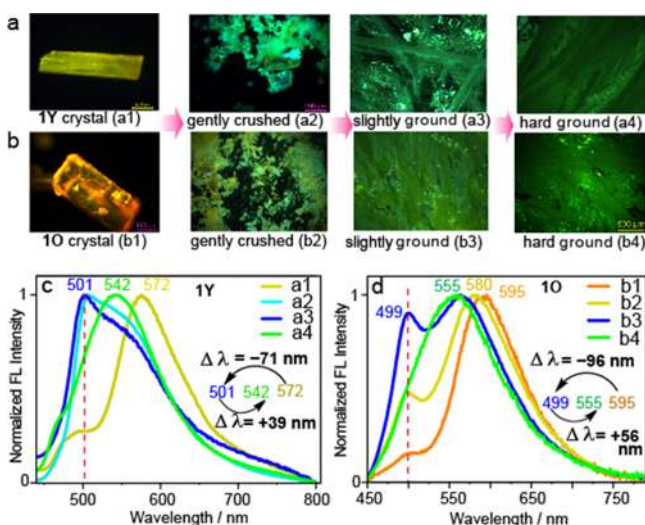
Figure 2. Fluorescence microscopy images and corresponding spectra of multistage mechanochromic luminescence. (a) **1Y** crystal and (b) **1O** crystal. The stepwise color changes are given in subpanels (a1−a4) and (b1−b4). (c) Fluorescence spectra for **1Y** in different stages of grinding with reference to (a1−a4). (d) Fluorescence spectra for **1O** crystals with reference to (b1−b4).

interaction in ordered crystalline state (Figure S8a, SI). Moreover, excitation wavelength-dependent emission studies of **1O** also substantiate the claim that intermolecular interaction in crystalline state is responsible for bathochromic shift of fluorescence band. As the excitation wavelength increases from 460 to 523 nm, the emission gradually red-shifted (Figure S8b,c, SI).[59] Similarly, the excitation maximum at ∼500 nm, which corresponds to intermolecular interaction, gradually red-shifted with increasing the monitoring wavelength (Figure S8d). All of these observations validate the presence of intermolecular charge-transfer interaction in the crystalline state. In addition to the crystals, the PL color of **1** can also be tuned by simply embedding in a different polymer matrix (5 wt % of **1** from dimethylformamide (DMF) solution of the polymer) having different functional groups (Figure S9, SI). Variation of the fluorescence color was observed depending on the intermolecular interaction between the molecules of **1** and the functional groups of the polymer matrix.

Interestingly, the crystals of **1Y** and **1O** display a unique multistage mechanochromic response that exhibits "back and forth" PL wavelength switching. With gradual increase of mechanical pressure (careful hand grinding by mortar and pestle), both the pristine crystals show initial hypsochromic PL shift, followed by bathochromic PL shift. Specifically, gentle crushing of the pristine **1Y** crystal (a1 and a2, Figure 2a) and **1O** crystal (b1 and b2, Figure 2b) triggers the formation of cyan emissive form with prominent rise of the emission peak at 501 nm (for **1Y**, $\Delta\lambda_{em} = -71$ nm) or 499 nm (for **1O**, $\Delta\lambda_{em} = -96$ nm) (Figure 2c,d). Further increase of grinding pressure leads to the green emissive film having emission band at $\lambda_{em,max} = 542$ nm for **1Y**-ground film (a3 and a4, Figure 2a) and 555 nm for **1O**-ground film (b2−b4, Figure 2b). Experimental powder X-ray diffraction (PXRD) plot of **1O**-ground powder and **1Y**-ground powder shows similar pattern with small difference in peak position (Figure S10, SI). This suggests that grinding of both the crystals leads to green emissive forms that have similar molecular arrangements and electronic interactions. To the best of our knowledge, **1O** or **1Y** is the first

example of a purely organic material that shows such unique mechanochromic luminescence behavior. Moreover, large blue-shifted mechanochromic luminescence (with overall $\Delta\lambda_{em} = +(40-58$ nm)) is another important feature of our system. It is important to note that, compared to red-shifted mechano-fluorochromism in solid organic materials, the examples of blue-shifted ones are rather very limited.[47−51]

To obtain a deeper insight into the structure function correlation, we have carried out single-crystal X-ray diffraction of the luminescent crystals. Orange emissive form **1O** crystallizes in triclinic system with centrosymmetric $P\bar{1}$ space group (Figure 3 and Table S2, SI), consisting of three
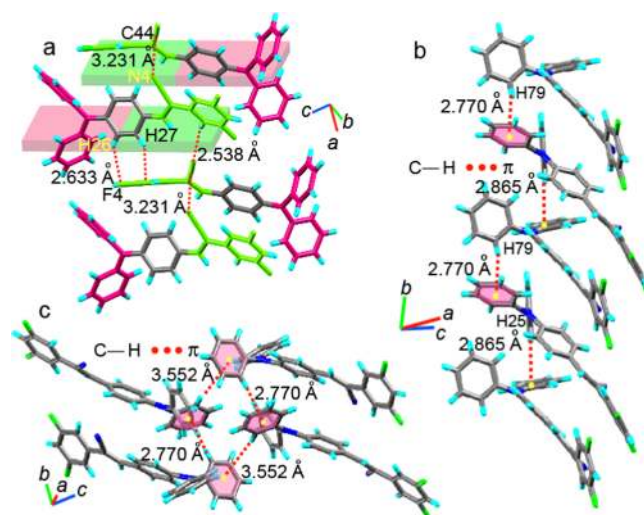

Figure 3. (a) Intermolecular interactions in the crystal structure of **1O**. Arrangement of donor−acceptor groups are colored red and green, respectively. (b, c) C−H···π interactions along different crystallographic directions.

molecules in asymmetric unit. Out of three, two molecules lie parallel in a slip-stacked fashion having a longitudinal slipping angle of 46.07° and a distance of 5.295 Å (between two acceptor phenyl planes). The other molecule in the asymmetric unit lies antiparallel. Packing diagram reveals that the molecules are connected by hydrogen-bonding interactions involving aromatic protons and F or N atom of the neighboring molecules (C46−H46···F5, D−A distance = 3.238(3) Å; C26−H26···F4, distance = 3.399(3) Å; and C15−H15···N6, distance = 3.259(4) Å). In addition to these interactions, several C−H···π interactions (H to centroid distances of 2.770 and 2.865 Å) were also observed that connect the molecules in different crystallographic directions (Figures 3b,c, S11, S12, and Table S3, SI). These interactions provide rigidity to the molecule in packed solid state and reduce the nonradiative decay that enhance fluorescence quantum yield (QY) in crystal (compared to solution).[60−62] Notably, π−π interactions were not observed in the crystal structure possibly because of the bulkiness and nonplanar orientation of triphenyl moiety that restrict closure vicinity of the molecules.[35,60,61,63] This is another reason for QY enhancement of **1** in the solid state (Table S1, SI), since π−π interaction is known to impart detrimental effect on fluorescence intensity. Our repeated attempts to obtain good X-ray-quality crystals of yellow emissive and green emissive form were unsuccessful. A comparative look at the PXRD plots reveals that the majority of the peaks in **1O**-ground form has slightly higher 2θ values than others, indicating relatively denser
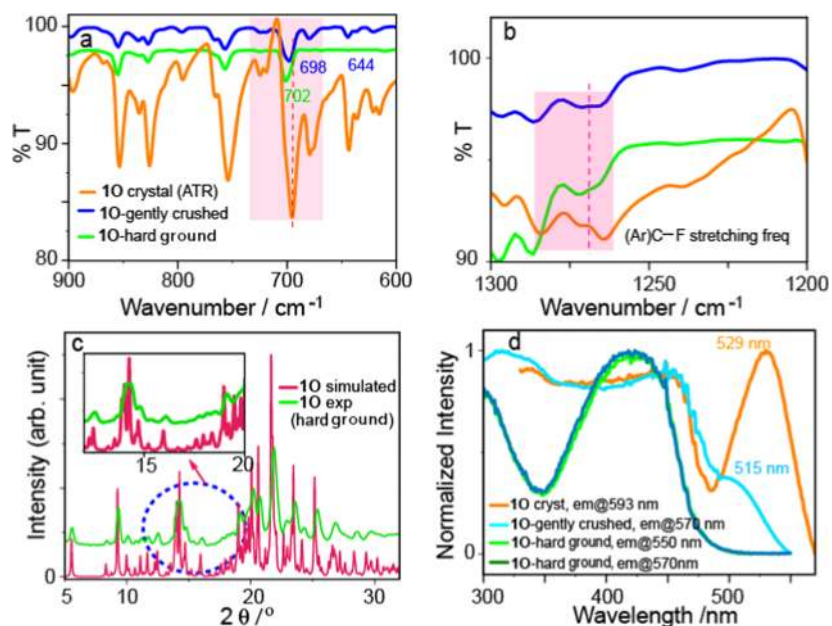
Figure 4. (a) Comparative IR spectra (attenuated total reflection) of pristine **1O** crystal, gently crushed, and hard ground powder. (b) Changes in aromatic C−F stretching frequency modes. The color legends shown in (a) apply for (b) as well. (c) Overlay PXRD pattern of experimental (hard ground powder) and simulated (from single crystal) **1O**. Simulated patterns were obtained from the crystal structure using Mercury software version 3.7. (d) Fluorescence excitation spectra at different stages of grinding of **1O** crystal.

packing in pristine **1O** crystal, which favors stronger intermolecular interactions that facilitate bathochromic shift of fluorescence emission (Figure S12b).

To elucidate the mechanism of distinct mechanochromic luminescence of **1Y** and **1O** crystals, we have carried out IR, Raman, PXRD, and fluorescence emission/excitation analyses at different stages of grinding. We hypothesized that multistage mechanochromism could arise from the pressure-induced rotational dynamics of phenyl groups that lead to conformational change of the molecule and affect the intermolecular charge-transfer interaction (Table S4, SI). Infrared spectra of **1O** crystal, **1O**-gently crushed, and **1O**-hard ground green emissive film showed distinct features of aromatic C−H bond frequency (stretching, in-plane, and out-of-plane vibrations; Figures 4a,b and S13, SI). This suggests that the symmetry and conformation of the molecules have changed during the course of grinding. Particularly, the blue shift of out-of-plane bending frequency at 698 cm^{-1} (Figure 4a) and in-plane bending frequency at 1270 cm^{-1} (Figure S13b) indicates that grinding leads to weakening of the intermolecular interactions involving aromatic C−H bonds. The upshift of C≡N stretching frequency upon grinding suggests the strengthening of C≡N bond and weakening of intermolecular interaction involving this group (Figure S13d, SI). Moreover, the slight blue shift of aromatic C−F bond stretching frequency indicates that intermolecular hydrogen-bonding interactions involving C−F···H moiety become weaker in ground state (Figures 4b, S14a, and Table S3, SI). Such weakening of intermolecular interaction in solid state would result in the loss of crystallinity and long-range order. In fact, PXRD of the hard ground green emissive powder of **1O** exhibits broader reflection peaks compared to the simulated one (obtained from single-crystal **1O**, Figure 4c), which also supports the above statement.

Furthermore, as observed from Figure 4d, fluorescence excitation spectra of the **1O** crystal, **1O**-gently crushed, and **1O**-hard ground film are different, suggesting the involvement

of distinct electronic states that are responsible for emission switching. Specifically, upon increasing the grinding pressure, the intermolecular interaction band at λ_{max} = 529 and 515 nm disappeared along with blue shift of the ICT band. This intermolecular interaction band in the ca. 500−550 nm region is not present in the absorption spectra of **1O**-hard ground film, in line with the above observation (Figure S14b, SI). In contrast to **1O** crystal, the excitation wavelength-dependent emission spectra of **1O**-hard ground film do not display red shift of the emission band upon increasing the excitation wavelength (Figure S14c, SI). All of these results justify that grinding leads to the loss of long-range intermolecular interaction. The excitation spectra of **1Y** crystal also reflect the same trend (as in case of **1O**), suggesting similar change in electronic states at different stages of grinding (Figure S14d, SI). Fluorescence lifetime study at different stages of the grinding reveals that lifetime decreases upon gentle crushing to metastable cyan emitting state and again slightly increases for hard ground green emissive film, which is more stable (Table S5 and Figure S15, SI).

On the basis of all of these experimental observations, we suggest a mechanistic model of unique mechanochromic luminescence of **1O** and **1Y** crystals (Figure 5). The yellow or orange emission of the crystal is dominated by long-range
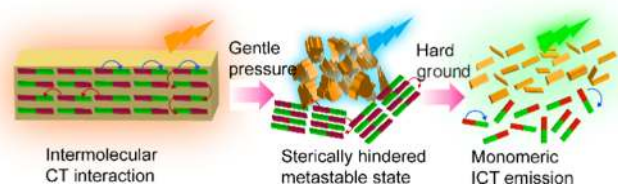

Figure 5. Possible mechanism of supramolecular rearrangement of D−A molecules (shown as red-green bicolor rods) at different stages of grinding. Luminescence color at each stage is also shown.

order that facilitate intermolecular charge-transfer interactions. Application of gentle pressure (on 001 face, as observed from BDFH analysis and molecular arrangement; Figure S16, SI) changes molecular orientation by reconfiguration of weak intermolecular interactions. This leads to a sterically congested metastable state, where nonradiative decay is restricted and thus exhibits hypsochromically shifted cyan emission. Further increase of grinding pressure (hard ground green emissive film) leads to randomization of molecules and diminution of long-range order, where monomeric ICT green emission is prevalent.

Next, we have tested the morphology-dependent emission behavior of **1** in crystalline and amorphous states. **1** drop-cast from DMF solution (1×10^{-3} M) produced well-shaped microcrystalline architecture (Figure 6a), which emits yellow
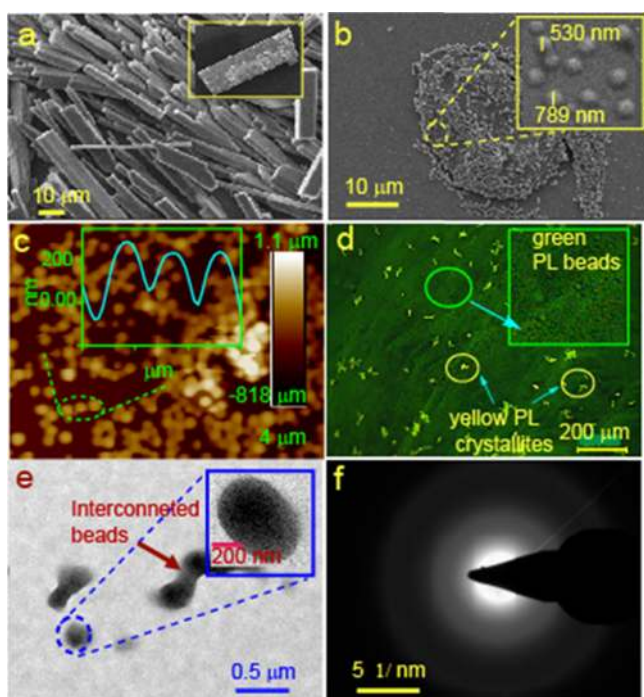

Figure 6. (a) SEM image of crystallites of **1** obtained by drop casting from DMF solution. (b, c) SEM and atomic force microscopy (AFM) images of bead-shaped particles of **1** from methanol solution. (d) Fluorescence microscopy image of drop-cast (from methanol) solid; amorphous beads show green fluorescence and crystallites show yellow fluorescence. (e) TEM image of beads and (f) selected area electron diffraction (SAED) image of the bead particles.

fluorescence. When drop-cast from methanol (1×10^{-3} M), it formed green fluorescent beadlike particles with average dimension of 500−800 nm radius and 200−300 nm height, along with some small crystallites (Figure 6b−d). As observed by scanning electron microscopy (SEM) and transmission electron microscopy (TEM), some interconnected beads were also formed. Selected area electron diffraction (SAED) image confirmed that green fluorescent beads are amorphous in nature (Figure 6f). Moreover, fluorescence microscopy reveals that amorphous beads are green emissive and small crystallites are yellow emissive (Figure 6d). This suggests that green emission is contributed by monomeric ICT interaction, where molecules are randomly oriented without having strong intermolecular interactions. On the contrary, long-range order in crystalline state facilitates intermolecular charge-transfer

interaction, which results in red-shifted emission. This observation is in accordance with our proposed mechanism for mechanochromic luminescence.

The unique mechanochromic behavior of **1Y** and **1O** crystals motivated us to explore their response to other stimuli, such as solvent vapors or heat. A general schematic diagram of multistimuli-responsive behavior is depicted in Figure 7.
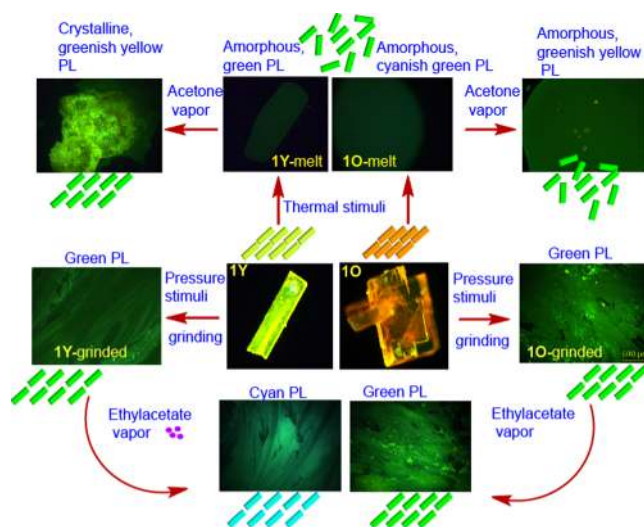

Figure 7. Multistimuli (pressure-, vapo-, thermo-) responsive behavior and possible changes in the molecular arrangement in **1O** and **1Y** crystal/powder.

Interestingly, compound **1** exhibits pronounced vapochromic and thermochromic fluorescence switching (Figures S17−S21, SI). When **1Y**-ground film (green emissive, λ_{max} = 540 nm) was exposed to ethyl acetate vapor or benzene vapor, it showed notable vapochromic swing to cyan emission (λ_{max} = 498 nm, Figure S17, SI). A similar phenomenon was also observed for **1O**-ground film, however, much weaker in response (Figure S18, SI). In contrast to the ground film, the pristine crystals do not show such vapochromic response, possibly because of the compact packing of the molecules. Void space calculation on the crystal structure of **1O** reveals no accessible void space that can accommodate solvent molecules. However, in the ground film state, molecules are more disordered, loosely packed, and spaced. TGA of vapor-exposed ground sample did not show any solvent loss, which discards the possibility of solvent trapping. Thus, possible mechanism of vapochromic response can be explained in terms of vapor-induced rearrangement of molecules. The interaction of solvent vapor with the disordered molecules of **1Y**-ground film allows them to relax to a different type of packing.

The effect of thermal stimuli on these solid emitters was studied by TGA, DSC, and hot-stage fluorescence microscopy (Figures S4, S5, and S19−S21, SI). Heating of all of the crystals **1Y** and **1O** to melt state leads to the loss of fluorescence and crystallinity. However, upon cooling to room temperature (RT), the solidified material showed very weak green emission (λ_{max} =548 nm). PXRD study confirmed that these melt-solidified materials are amorphous (Figure S20c and S21b). Interestingly, upon exposure to acetone vapor at room temperature, amorphous melt compound (**1Y**-melt or **1O**-melt, Figures S20 and S21, SI) regains its crystallinity with slight shift in fluorescence wavelength to greenish yellow. At the initial stage of crystallization/nucleation (red-shaded region
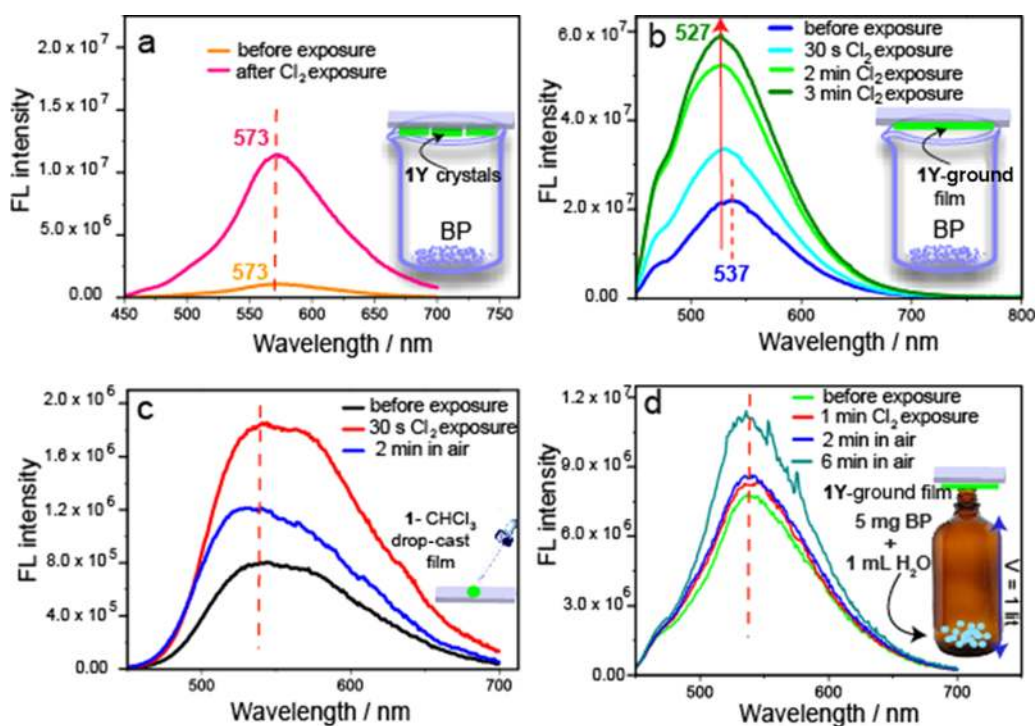
Figure 8. Chlorine gas (evolved from bleaching powder and water) sensing by **1**. (a) PL spectral change of **1Y** crystal before and after exposure. Bleaching powder is abbreviated as BP in the figure panels. (b, c) Same for **1Y**-ground film and **1** drop-cast film (from chloroform solution). (d) **1Y**-ground film with approximately 1.7 ppm (in air) chlorine concentration.

in Figure S20d, SI), the PL intensity is decreased, but recovered its moderate intensity after exposing to air for 3−10 min of crystallization.

The promising vaporesponsive property of **1Y** and **1O** in solid state prompted us to utilize them as a sensor for harmful gases like chlorine. Exposure of solid crystals of **1Y** to chlorine gas (from commercially available bleaching powder with addition of small amount of water) leads to significant increase in PL intensity (Figure 8a). **1Y** crystal showed 11-fold increase in intensity when exposed to chlorine gas released from 20 mg of bleaching powder (35%). Not only crystal but also the ground and drop-cast films (from chloroform solution) act as sensor for chlorine gas (Figure 8b,c). The sensing of ground or drop-casted film is not fully reversible. Keeping the material in air for 30 min or heating at 50 °C for 10 min leads to the decrease in PL intensity, but does not return to its original emission intensity. This irreversibility was also observed from ^{1}H NMR study (discussed later).

To test the efficiency of the sensing, we have carried out few experiments using different amounts of bleaching powder in constant air volume of 1 L (Figure 8d).[a] **1Y**-ground film exhibited a slight increase in PL intensity when exposed to low concentration of chlorine gas, suggesting the strong sensing ability of the same. The response is dependent on the concentration of chlorine gas. As shown in Figure S22 (SI), the PL intensity gradually increases with increasing the chlorine gas concentration from 5 to 10 ppm.

To elucidate the mechanism of chlorine gas sensing, we have carried out few experiments before and after chlorine gas exposure. The changes observed from PXRD and IR spectroscopy (Figures S23 and S24, SI) suggest the negligible change in supramolecular rearrangement. Interestingly, similar to solid-state behavior, the solution of **1** (in CHCl$_3$) when purged with chlorine gas also showed increase in fluorescence intensity with

a slight shift in wavelength. This suggests possible charge-transfer interaction between **1** and chlorine, although the possibility of chemical reaction cannot be ruled out. ^{1}H NMR spectra at different stages of chlorine gas purging showed prominent change in the 7.10−6.70 ppm region with the rise of several triplet peaks, suggesting o-chlorination of DPA ring (Figure S26). This change is irreversible even after heating the solution at 50 °C for 10 min or keeping the solution at RT for 48 h. Mass spectra showed a peak at 478.206, which corresponds to dichlorinated product of **1** (Figure S27, SI). On the basis of all of the above observations, we believe that the initial increase in fluorescence intensity is due to donor−acceptor-type interaction of **1** with chlorine gas, which diminishes after certain time when chlorination of the DPA moiety starts. Precise study with pure chlorine gas tank equipped with ppm-level sensor is out of our reach and beyond the scope of this study. However, details of solid-state sensing experiments and its mechanistic process are currently under investigation in our lab and will be part of future study.

■ CONCLUSIONS

In summary, we have developed a synthetically simple molecular material that exhibits unique mechanochromic luminescence, i.e., "back and forth" wavelength switching at different stages of mechanical grinding. The interplay between intermolecular charge transfer facilitated by long-range order in crystal and intramolecular charge-transfer interaction in powder is responsible for such fluorescence switching. We have also developed a mechanistic model that successfully explains this unusual mechanofluorochromism. Moreover, we have demonstrated that the same material can be used as a solid-state sensor for harmful chlorine gas. Unlike multistep synthesis and tedious purification process, this material was obtained in pure form by one-step reaction, followed by recrystallization, and thus poses

advantage in terms of cost effectiveness and practical usability. Such concept design of molecule can be exploited further to develop new materials having distinct optical property that can be used for sensory and optoelectronic application.

■ EXPERIMENTAL SECTION

General Information. *Materials and Methods.* 4-(Diphenylamino)benzaldehyde was purchased from Sigma-Aldrich and used without further purifications. 3,5-Difluorobenzyl cyanide was purchased from TCI India and used as received. Tetrabutyl ammonium hydroxide (TBAH) was obtained from Spectrochem and used as received. Laboratory-grade solvents were used for the synthesis, and spectroscopy-grade solvents were used for crystallization and spectroscopy studies.

Instrument Details. NMR. ^{1}H NMR (500 MHz) and ^{13}C NMR (125 MHz) spectra were recorded on a Bruker ASCEND 500 spectrometer using $CDCl_3$ as solvent. The chemical shifts (δ) are given in ppm and referenced to the internal standard tetramethylsilane $(Si(CH_3)_4)$.

Mass Spectra. High-resolution mass spectra of the compound were recorded on a Thermo Scientific Exactive Benchtop LC/HRMS Orbitrap mass spectrometer in the electrospray ionization (ESI) (SI) mode.

UV−Vis Spectra. Solution-state UV−vis absorption spectra were recorded on a Shimadzu UV-2600 spectrophotometer, and solid-state absorption spectra were recorded on a PerkinElmer Lambda 35 UV−vis spectrophotometer.

Emission Spectra. Solid-state emission spectra of the crystals and ground samples were recorded on a HORIBA SPEX Fluorolog spectrofluorometer FL-1039. The crystals or ground samples were glued on the quartz plate with nonfluorescent grease placed on optical path, and spectra were recorded in front face mode. Solution-state quantum yield of **1** (in chloroform) was calculated by standard procedure[64] using fluorescein dye as standard sample (QY in ethanol is 0.79). For absolute quantum yields (QYs) measurement, the crystals and ground samples were sandwiched between two glass plates placed in the optical path inside a calibrated integrating sphere in a HORIBA Fluorolog spectrofluorometer (SPEX) employing a Xe arc lamp as excitation source in the sphere using specific excitation wavelengths. Prior to the experiment, the integrating sphere was calibrated using tris(8-hydroxyquinolinato)-aluminum. The absolute quantum yield was calculated using the method reported previously.[65] Fluorescence image were captured using a Leica DM 2500P microscope equipped with Linkam THMS600 hot stage.

Fluorescence Lifetime. Fluorescence lifetime measurements were performed on a Leica TCS SP8 instrument.

IR Spectra. Infrared spectra were recorded on a SHIMADZU IR Prestige-21 spectrometer using KBr as matrix.

Raman Spectra. The crystals and ground film were recorded using a WiTec α-300R Confocal Raman microscope.

DSC and TGA. Differential scanning calorimetry (DSC) measurements were carried out on a TA Instruments DSC Q2000 model with a Peltier cooling system with a heating and cooling rate of 10 °C/min under nitrogen atmosphere. Thermogravimetric analyses (TGA) were performed on a TA Instruments SDT Q600 V20.9 Build 20, with a heating rate of 10 °C/min using nitrogen (50 mL/min) as purging gas.

SEM and TEM. Scanning electron microscopy (SEM) images were obtained from JEOL-JSM5610 instrument using 8−10 kV energy. Samples were prepared by drop casting from methanol

or DMF solution on silicon wafers and dried at ambient temperature. The samples were coated with gold prior to the SEM study. Transmission electron microscopy (TEM) measurements were performed on an FEI Tecnai T30 system with EDAX microscope at an accelerating voltage of 300 kV. The samples were prepared by drop casting from methanol solution of **1** on a carbon-coated copper grid. Atomic force microscopy (AFM) measurements were carried out with Bruker NanoScope instrument with a nominal tip (Veeco RTESP tips, 1−10 Ω/cm), phosphorus doped Si was used as cantilevers at the resonant frequency range of 266−326 kHz. Scan arrays were 256 × 256 points, and the scan rate was 0.62 Hz.

PXRD. Powder X-ray diffraction (PXRD) was measured by a XEUSS SAXS/WAXS system by Xenocs, operated at 50 kV and 0.60 mA. The X-ray radiation was collimated with FOX2D mirror and two pairs of scatterless slits from Xenocs. The data were collected in the transmission mode geometry using Cu Kα radiation (wavelength λ = 1.54 Å). The fiber diagrams were recorded using an image plate system (mar345 detector) and processed using FIT2D software.

Single-Crystal X-ray Diffraction. The data of **1O** crystal were collected on a Bruker APEX-II CCD diffractometer at 298 K using graphite-monochromated Mo Kα radiation (λ = 0.71069 Å). Data reduction was carried out with SAINT software and analyzed for agreement using XPREP.[66] Absorption correction was carried out with the SADABS program.[67] The structure was determined by the method included in SHELXT program of the APEX software suite and refined using SHELXL-2014.[68−71] The nonhydrogen atoms were refined anisotropically. Details of crystallographic parameters are given in Table S2, Supporting Information. The crystallographic data have been deposited with the Cambridge Crystallographic Data Centre under references 1564351 (**1O**).

Computational Methods. All of the theoretical calculations were carried out using the Gaussian 098 program suite. Density functional theory (DFT) with hybrid B3LYP functionals[72−74] and the 6-31G(d) basis sets were used for gas-phase geometry optimization of compound **1** using coordinates from crystal structure (**1O**) as input. Tomasi's polarizable continuum model (PCM)[75] was used for describing the solvent effect on the HOMO−LUMO gap of the compound. All of the output structures were visualized by Chemcraft software.

Synthetic Procedure. A 100 mL round-bottom flask equipped with a magnetic stirrer and reflux condenser was charged with 4-(diphenylamino)benzaldehyde (0.238 g, 0.87 mmol) and 3,5-difluorobenzyl cyanide (0.1 mL, 0.87 mmol) in 30 mL of methanol solution. Potassium *tert*-butoxide (0.112 g, 1.0 mmol) and tetrabutyl ammonium hydroxide (25% methanol solution, 1 mL, 1.0 mmol) were added to the flask, and the resulting mixture was heated at 80 °C for 5 h. The product mixture was cooled and kept for crystallization for 3 days. Yellow crystalline product was obtained from mother liquor, which was isolated by filtration (0.285 g, 80%). ^{1}H NMR (500 MHz, $CDCl_3$): δ (ppm) 7.77 (d, 2H, Ar−H, J = 8 Hz), 7.42 (s, 1H, Ar−H), 7.33 (t, 4H, Ar−H, J = 8 Hz), 7.15−7.18 (m, 8H, Ar−H), 7.03 (d, 2H, Ar−H, J = 8 Hz), 6.79 (t, 1H, Ar−H, J = 8 Hz). ^{13}C NMR (125 MHz, $CDCl_3$) δ (ppm) 164.44, 162.47, 150.72, 146.4, 143.37, 138.5, 131.14, 129.66, 125.98, 125.3, 124.77, 120.36, 118.07, 108.75, 108.54, 105.19, 103.89, 103.72, 103.51. HRMS: m/z = 409.15199 (M + H), calcd (M + H) for $C_{27}H_{18}F_2N_2$ is 409.1516. Elemental analysis: calcd for $C_{27}H_{18}F_2N_2$: C: 79.40; H: 4.44; N: 6.86; obtained: C:

79.68; H: 4.437; N: 6.89. HRMS for **1Y** m/z = 409.1519, **1O**, m/z = 409.1518.

ASSOCIATED CONTENT

Supporting Information

The Supporting Information is available free of charge on the ACS Publications website at DOI: 10.1021/acsomega.8b00250.

AUTHOR INFORMATION

Corresponding Authors

*E-mail: mbalaram@iiserkol.ac.in. Tel: +91-9748-261 742, +91-33-2587 3020 (B.M.).

*E-mail: mannup25@gmail.com, manas.panda@niist.res.in. Tel: +91 471-253-5608 (M.K.P.).

ORCID

Manas K. Panda: 0000-0002-6297-2070

Author Contributions

$^\nabla$A.A. and T.P. contributed equally to this manuscript.

Notes

The authors declare no competing financial interest.

ACKNOWLEDGMENTS

ADDITIONAL NOTE

^{a}Considering that commercial bleaching powder have 35% active chlorine, we can approximately estimate the concentration of chlorine gas (in ppm) that is released upon addition of small amount of water. For example, if 1 mL of water was added to 5 mg of bleaching powder that is kept inside a 1 L bottle (Figure 8d), then we can assume that the concentration of released chlorine gas that occupies 1 L volume is 1.7 ppm (1.75 mg of active chlorine gas per 1 L air volume). Considering that chlorine gas is heavier than air, the actual concentration at the top of the bottle might be lower than 1.7 ppm.

REFERENCES

(1) Farinola, G. M.; Ragni, R. Electroluminescent materials for white organic light emitting diodes. *Chem. Soc. Rev.* **2011**, *40*, 3467−3482.

(2) Shimada, M.; Tsuchiya, M.; Sakamoto, R.; Yamanoi, Y.; Nishibori, E.; Sugimoto, K.; Nishihara, H. Bright Solid-State Emission of Disilane-Bridged Donor-Acceptor-Donor and Acceptor-Donor-Acceptor Chromophores. *Angew. Chem., Int. Ed.* **2016**, *55*, 3022−3026.

(3) Li, C.; Hanif, M.; Li, X.; Zhang, S.; Xie, Z.; Liu, L.; Yang, B.; Su, S.; Ma, Y. Effect of cyano-substitution in distyrylbenzene derivatives on their fluorescence and electroluminescence properties. *J. Mater. Chem. C* **2016**, *4*, 7478−7484.

(4) Xue, J.; Li, C.; Xin, L.; Duan, L.; Qiao, J. High-efficiency and low efficiency roll-off near-infrared fluorescent OLEDs through triplet fusion. *Chem. Sci.* **2016**, *7*, 2888−2895.

(5) Ghosh, S.; Philips, D. S.; Saeki, A.; Ajayaghosh, A. Nanosheets of an Organic Molecular Assembly from Aqueous Medium Exhibit High Solid-State Emission and Anisotropic Charge-Carrier Mobility. *Adv. Mater.* **2017**, *29*, No. 1605408.

(6) Park, S. K.; Kim, J. H.; Yoon, S. J.; Kwon, O. K.; An, B. K.; Park, S. Y. High-Performance n-Type Organic Transistor with a Solution-Processed and Exfoliation-Transferred Two-Dimensional Crystalline Layered Film. *Chem. Mater.* **2012**, *24*, 3263−3268.

(7) Hirata, S.; Lee, K.; Watanabe, T. Reversible Fluorescent On-Off Recording in a Highly Transparent Polymeric Material Utilizing Fluorescent Resonance Energy Transfer (FRET) Induced by Heat Treatment. *Adv. Funct. Mater.* **2008**, *18*, 2869−2879.

(8) Pu, S.; Tang, H.; Chen, B.; Xu, J.; Huang, W. Photochromic diarylethene for two-photon 3D optical storage. *Mater. Lett.* **2006**, *60*, 3553−3557.

(9) Cheng, X.; Wang, K.; Huang, S.; Zhang, H.; Zhang, H.; Wang, Y. Organic Crystals with Near-Infrared Amplified Spontaneous Emissions Based on 2′-Hydroxychalcone Derivatives: Subtle Structure Modification but Great Property Change. *Angew. Chem., Int. Ed.* **2015**, *54*, 8369−8373.

(10) Camposeo, A.; Polo, M.; Carro, P. D.; Silvestri, L.; Tavazzi, S.; Pisignano, D. Random lasing in an organic light-emitting crystal and its interplay with vertical cavity feedback. *Laser Photonics Rev.* **2014**, *8*, 785−791.

(11) Fang, H.; Chen, Q.; Yang, J.; Xia, H.; Gao, B.; Feng, J.; Ma, Y.; Sun, H. Two-Photon Pumped Amplified Spontaneous Emission from Cyano-Substituted Oligo(p-phenylenevinylene) Crystals with Aggregation-Induced Emission Enhancement. *J. Phys. Chem. C* **2010**, *114*, 11958−11961.

(12) Thirumalai, R.; Mukhopadhay, R. D.; Praveen, V. K.; Ajayaghosh, A. A slippery molecular assembly allows water as a self-erasable security marker. *Sci. Rep.* **2015**, *5*, No. 9842.

(13) Kumar, P.; Dwivedi, J.; Gupta, B. K. Highly luminescent dual mode rare-earth nanorod assisted multi-stage excitable security ink for anti-counterfeiting applications. *J. Mater. Chem. C* **2014**, *2*, 10468−10475.

(14) Sonawane, S. L.; Asha, S. K. Fluorescent Cross-Linked Polystyrene Perylenebisimide/Oligo(p-Phenylenevinylene) Microbeads with Controlled Particle Size, Tunable Colors, and High Solid State Emission. *ACS Appl. Mater. Interfaces* **2016**, *8*, 10590−10599.

(15) Basta, A.; Missori, M.; Girgis, A. lS.; De Spirito, M.; Papie, M.; El-Saied, H. Novel fluorescent security marker. Part II: application of novel 6-alkoxy-2-amino-3,5-pyridinedicarbonitrile nanoparticles in safety paper. *RSC Adv.* **2014**, *4*, 59614−59625.

(16) Lu, H.; Zheng, Y.; Zhao, X.; Wang, L.; Ma, S.; Han, X.; Xu, X.; Tian, W.; Gao, H. Highly Efficient Far Red/Near-Infrared Solid Fluorophores: Aggregation-Induced Emission, Intramolecular Charge Transfer, Twisted Molecular Conformation, and Bioimaging Applications. *Angew. Chem., Int. Ed.* **2016**, *55*, 155−159.

(17) Liu, J.; Chen, C.; Ji, S.; Liu, Q.; Ding, D.; Zhao, D.; Liu, B. Long wavelength excitable near-infrared fluorescent nanoparticles with aggregation-induced emission characteristics for image-guided tumor resection. *Chem. Sci.* **2017**, *8*, 2782−2789.

(18) Rong, G.; Corrie, S. R.; Clark, H. A. In Vivo Biosensing: Progress and Perspectives. *ACS Sens.* **2017**, *2*, 327−338.

(19) Rajamalli, P.; Gandeepan, P.; Huang, M.; Cheng, C. Bromo induced reversible distinct color switching of a structurally simple

donor-acceptor molecule by vapo, piezo and thermal stimuli. *J. Mater. Chem. C* **2015**, *3*, 3329−3335.

(20) Yoon, S. J.; Park, S. Y. Polymorphic and mechanochromic luminescence modulation in the highly emissive dicyanodistyrylbenzene crystal: secondary bonding interaction in molecular stacking assembly. *J. Mater. Chem.* **2011**, *21*, 8338−8346.

(21) Ongungal, R. M.; Sivadas, A. P.; Kumar, N. S. S.; Menon, S.; Das, S. Self-assembly and mechanochromic luminescence switching of trifluoromethyl substituted 1,3,4-oxadiazole derivatives. *J. Mater. Chem. C* **2016**, *4*, 9588−9597.

(22) Hariharan, P. S.; Moon, D.; Anthony, S. P. Reversible fluorescence switching and topochemical conversion in an organic AEE material: polymorphism, defection and nanofabrication mediated fluorescence tuning. *J. Mater. Chem. C* **2015**, *3*, 8381−8388.

(23) Zhao, Y.; Gao, H.; Fan, Y.; Zhou, T.; Su, Z.; Liu, Y.; Wang, Y. Thermally Induced Reversible Phase Transformations Accompanied by Emission Switching Between Different Colors of Two Aromatic-Amine Compounds. *Adv. Mater.* **2009**, *21*, 3165−3169.

(24) Xue, P.; Chen, P.; Jia, J.; Xu, Q.; Sun, J.; Yao, B.; Zhang, Z.; Lu, R. A triphenylamine-based benzoxazole derivative as a high-contrast piezofluorochromic material induced by protonation. *Chem. Commun.* **2014**, *50*, 2569−2571.

(25) Li, M.; Zhang, Q.; Wang, J.; Mei, X. Mechanochromism triggered fluorescent color switching among polymorphs of a natural fluorescence pigment. *Chem. Commun.* **2016**, *52*, 11288−11291.

(26) Kui, S. C. F.; Chui, S. S.-Y.; Che, C.-M.; Zhu, N. Structures, Photoluminescence, and Reversible Vapoluminescence Properties of Neutral Platinum(II) Complexes Containing Extended π-Conjugated Cyclometalated Ligands. *J. Am. Chem. Soc.* **2006**, *128*, 8297−8309.

(27) Bai, L.; Bose, P.; Gao, Q.; Li, Q.; Ganguly, R.; Zhao, Y. Halogen-Assisted Piezochromic Supramolecular Assemblies for Versatile Haptic Memory. *J. Am. Chem. Soc.* **2017**, *139*, 436−441.

(28) Davis, R.; Rath, N. P.; Das, S. Thermally reversible fluorescent polymorphs of alkoxy-cyano-substituted diphenylbutadienes: role of crystal packing in solid state fluorescence. *Chem. Commun.* **2004**, 74−75.

(29) Peterson, G. I.; Larsen, M. B.; Ganter, M. A.; Storti, D. W.; Boydston, A. J. 3D-Printed Mechanochromic Materials. *ACS Appl. Mater. Interfaces* **2015**, *7*, 577−583.

(30) Chi, Z.; Zhang, X.; Xu, B.; Zhou, X.; Ma, C.; Zhang, Y.; Liu, S.; Xu, J. Recent advances in organic mechanofluorochromic materials. *Chem. Soc. Rev.* **2012**, *41*, 3878−3896.

(31) An, B. K.; Gihm, S. H.; Chung, J. W.; Park, C. R.; Kwon, S. K.; Park, S. Y. Color-Tuned Highly Fluorescent Organic Nanowires/Nanofabrics: Easy Massive Fabrication and Molecular Structural Origin. *J. Am. Chem. Soc.* **2009**, *131*, 3950−3957.

(32) Toma, O.; Mercier, N.; Allain, M.; Meinardi, F.; Botta, C. Lead(II) 4,4′-Bipyridine N-Oxide Coordination Polymers-Highly Phosphorescent Materials with Mechanochromic Luminescence Properties. *Eur. J. Inorg. Chem.* **2017**, 844−850.

(33) Sun, Q.; Wang, H.; Xu, X.; Lu, Y.; Xue, S.; Zhang, H.; Yang, W. 9,10-Bis((Z)-2-phenyl-2-(pyridin-2-yl) vinyl)anthracene: Aggregation-induced emission, mechanochromic luminescence, and reversible volatile acids-amines switching. *Dyes Pigm.* **2018**, *149*, 407−414.

(34) Zhang, G.; Lu, J.; Sabat, M.; Fraser, C. L. Polymorphism and Reversible Mechanochromic Luminescence for Solid-State Difluoroboron Avobenzone. *J. Am. Chem. Soc.* **2010**, *132*, 2160−2162.

(35) Tan, R.; Lin, O.; Wen, Y.; Xiao, S.; Wang, S.; Zhanga, R.; Yi, T. Polymorphism and mechanochromic luminescence of a highly solid-emissive quinoline-β-ketone boron difluoride dye. *CrystEngComm* **2015**, *17*, 6674−6680.

(36) Guo, C.; Li, M.; Yuan, W.; Wang, K.; Zou, B.; Chen, Y. Tuning the Mechanochromic Luminescence of BOPIM Complexes by Rational Introduction of Aromatic Substituents. *J. Phys. Chem. C* **2017**, *121*, 27009−27017.

(37) Zhao, S.-S.; Chen, L.; Wang, L.; Xie, Z. Two tetraphenylethene-containing coordination polymers for reversible mechanochromism. *Chem. Commun.* **2017**, *53*, 7048−7051.

(38) Seki, T.; Takamatsu, Y.; Ito, H. A Screening Approach for the Discovery of Mechanochromic Gold(I) Isocyanide Complexes with Crystal-to-Crystal Phase Transitions. *J. Am. Chem. Soc.* **2016**, *138*, 6252−6260.

(39) Seki, T.; Jin, M.; Ito, H. Introduction of a Biphenyl Moiety for a Solvent-Responsive Aryl Gold(I) Isocyanide Complex with Mechanical Reactivation. *Inorg. Chem.* **2016**, *55*, 12309−12320.

(40) Seki, T.; Tokodai, N.; Omagari, S.; Nakanishi, T.; Hasegawa, S.; Iwasa, T.; Taketsugu, T.; Ito, H. Luminescent Mechanochromic 9-Anthryl Gold(I) Isocyanide Complex with an Emission Maximum at 900 nm after Mechanical Stimulation. *J. Am. Chem. Soc.* **2017**, *139*, 6514−6517.

(41) Park, S. K.; Cho, I.; Gierschner, J.; Kim, J. H.; Kim, J. H.; Kwon, J. E.; Kwon, O. K.; Whang, D. R.; Park, J.-H.; An, B.-K.; Park, S. Y. Stimuli-Responsive Reversible Fluorescence Switching in a Crystalline Donor-Acceptor Mixture Film: Mixed Stack Charge-Transfer Emission versus Segregated Stack Monomer Emission. *Angew. Chem., Int. Ed.* **2016**, *55*, 203−207.

(42) Kim, H.-J.; Whang, D. R.; Gierschner, J.; Lee, C. H.; Park, S. Y. High-contrast red-green-blue tricolor fluorescence switching in bicomponent molecular film. *Angew. Chem., Int. Ed.* **2015**, *54*, 4330−4333.

(43) Crenshaw, B. R.; Burnworth, M.; Khariwala, D.; Hiltner, A.; Mather, P. T.; Simha, R.; Weder, C. Deformation-Induced Color Changes in Mechanochromic Polyethylene Blends. *Macromolecules* **2007**, *40*, 2400−2408.

(44) Sagara, Y.; Kubo, K.; Nakamura, T.; Tamaoki, N.; Weder, C. Temperature-Dependent Mechanochromic Behavior of Mechanoresponsive Luminescent Compounds. *Chem. Mater.* **2017**, *29*, 1273−1278.

(45) Sagara, Y.; Simon, Y. C.; Tamaokia, N.; Weder, C. A mechano- and thermoresponsive luminescent cyclophane. *Chem. Commun.* **2016**, *52*, 5694−5697.

(46) Lavrenova, A.; Balkenende, D. W. R.; Sagara, Y.; Schrett, S.; Simon, Y. C.; Weder, C. Mechano- and Thermoresponsive Photoluminescent Supramolecular Polymer. *J. Am. Chem. Soc.* **2017**, *139*, 4302−4305.

(47) Nagura, K.; Saito, S.; Uasa, H.; Yamawaki, H.; Fujihisa, H.; Sato, H.; Shimoikeda, H.; Yamaguchi, S. Distinct Responses to Mechanical Grinding and Hydrostatic Pressure in Luminescent Chromism of Tetrathiazolylthiophene. *J. Am. Chem. Soc.* **2013**, *135*, 10322−10325.

(48) Tanioka, M.; Kamino, S.; Muranaka, A.; Ooyama, Y.; Ota, H.; Shirasaki, Y.; Horigome, J.; Ueda, M.; Uchiyama, M.; Sawada, D.; Enomoto, S. Reversible Near-Infrared/Blue Mechanofluorochromism of Aminobenzopyranoxanthene. *J. Am. Chem. Soc.* **2015**, *137*, 6436−6439.

(49) Wu, J.; Cheng, Y.; Lan, J.; Wu, D.; Qian, S.; Yan, L.; He, Z.; Li, X.; Wang, K.; Zou, B.; You, J. Molecular Engineering of Mechanochromic Materials by Programmed C-H Arylation: Making a Counterpoint in the Chromism Trend. *J. Am. Chem. Soc.* **2016**, *138*, 12803−12812.

(50) Suenaga, K.; Tanaka, K.; Chujo, Y. Heat-Resistant Mechano-luminescent Chromism of the Hybrid Molecule Based on Boron Ketoiminate Modified Octasubstituted Polyhedral Oligomeric Silsesquioxane. *Chem. — Eur. J.* **2017**, *23*, 1409−1414.

(51) Guo, K.; Zhang, F.; Guo, S.; Li, K.; Lu, X.; Li, J.; Wang, H.; Chenga, J.; Zhao, Q. Achieving red/near-infrared mechanoresponsive luminescence turn-on: mechanically disturbed metastable nanostructures in organic solids. *Chem. Commun.* **2017**, *53*, 1309−1312.

(52) Hui, W.; Jiaqiang, X.; Qingy, P. Synthesis and chlorine sensing properties of nanocrystalline hierarchical porous SnO$_2$ by a phenol formaldehyde resin-assisted process. *CrystEngComm* **2010**, *12*, 1280−1285.

(53) Saini, R.; Mahajan, A.; Bedi, R. K.; Aswal, D. K.; Debnath, A. K. Room temperature ppb level Cl$_2$ detection and sensing mechanism of highly selective and sensitive phthalocyanine nanowires. *Sens. Actuators, B* **2014**, *203*, 17−24.

(54) Xiang, F. High sensitivity chlorine gas sensors using $CdIn_2O_4$ thick film prepared by co-precipitation method. *Mater. Res. Bull.* **2003**, *38*, 1705−1711.

(55) Sultan, A.; Ahmad, S.; Mohammad, F. A highly sensitive chlorine gas sensor and enhanced thermal DC electrical conductivity from polypyrrole/silicon carbide nanocomposites. *RSC. Adv.* **2016**, *6*, 84200−84208.

(56) Baron, M. G.; Narayanaswamy, R.; Thorpe, S. C. A kineto-optical method for the determination of chlorine gas. *Sens. Actuators, B* **1995**, *29*, 358−362.

(57) Wu, Y. Y.; Chen, Y.; Gau, G. Z.; Mu, W. H.; Lv, X. J.; Du, M. L.; Fu, W. F. Large Stokes Shift Induced by Intramolcular Charge Transfer in N,O-Chelated Naphthyridine-BF_2 Complexes. *Org. Lett.* **2012**, *14*, 5226−5229.

(58) Yang, J.-S.; Liau, K.-L.; Wang, C.-M.; Hwang, C.-Y. Substituent-Dependent Photoinduced Intramolecular Charge Transfer in N-Aryl-Substituted trans-4-Aminostilbenes. *J. Am. Chem. Soc.* **2004**, *126*, 12325−12335.

(59) Huang, H. W.; Horie, K.; Yamashita, T.; Machida, S.; Sone, M.; Tokita, M.; Watanabe, J.; Maeda, Y. Fluorescence Study on Intermolecular Interactions between Mesogenic Biphenyl Moieties of a Thermotropic Liquid-Crystalline Polyester (PB-10). *Macromolecules* **1996**, *29*, 3485−3490.

(60) Yang, M.; Xu, D.; Xi, W.; Wang, L.; Zheng, J.; Huang, J.; Zhang, J.; Zhou, H.; Wu, J.; Tian, Y. Aggregation-Induced Fluorescence Behavior of Triphenylamine-Based Schiff Bases: The Combined Effect of Multiple Forces. *J. Org. Chem.* **2013**, *78*, 10344−10359.

(61) Han, T.; Feng, X.; Chen, D.; Dong, Y. A diethylaminophenol functionalized Schiff base: crystallization-induced emission-enhancement, switchable fluorescence and application for security printing and data storage. *J. Mater. Chem. C* **2015**, *3*, 7446−7454.

(62) He, Z.; Ke, C.; Tang, B. Z. Journey of Aggregation-Induced Emission Research. *ACS Omega* **2018**, *3*, 3267−3277.

(63) Zhao, X.; Xue, P.; Wang, K.; Chen, P.; Zhang, P.; Lu, R. Aggregation-induced emission of triphenylamine substituted cyanostyrene derivatives. *New J. Chem.* **2014**, *38*, 1045−1051.

(64) Lakowicz, J. R. *Principles of Fluorescence Spectroscopy*, 3rd ed.; Springer Science and Business Media, 2006; pp 9−10, 54−58.

(65) deMello, J. C.; Wittmann, H. F.; Friend, R. H. An improved experimental determination of external photoluminescence quantum efficiency. *Adv. Mater.* **1997**, *9*, 230−232.

(66) *APEX DUO*, version 2.1−4, and *SAINT*, version 7.34A; Bruker AXS Inc.: Madison, WI, 2012.

(67) Sheldrick, G. M. *SADABS*; University of Göttingen: Göttingen, Germany, 1996.

(68) Sheldrick, G. M. *SHELXL2014*; University of Göttingen: Göttingen, Germany, 2014.

(69) Sheldrick, G. M. *SHELXTL XT − Crystal Structure Solution*, version 2014/4; Bruker AXS, 2010−2014.

(70) Sheldrick, G. M. SHELXT − Integrated space-group and crystal-structure determination. *Acta Crystallogr. A* **2015**, *71*, 3−8.

(71) Sheldrick, G. M. A short history of SHELX. *Acta Crystallogr. A* **2008**, *64*, 112−122.

(72) Frisch, M. J.; Trucks, G. W.; Schlegel, H. B.; Scuseria, G. E.; Robb, M. A.; Cheeseman, J. R.; Scalmani, G.; Barone, V.; Mennucci, B.; Petersson, G. A.; Nakatsuji, H.; Caricato, M.; Li, X.; Hratchian, H. P.; Izmaylov, A. F.; Bloino, J.; Zheng, G.; Sonnenberg, J. L.; Hada, M.; Ehara, M.; Toyota, K.; Fukuda, R.; Hasegawa, J.; Ishida, M.; Nakajima, T.; Honda, Y.; Kitao, O.; Nakai, H.; Vreven, T.; Montgomery, J. A.; Peralta, J. E.; Ogliaro, F.; Bearpark, M.; Heyd, J. J.; Brothers, E.; Kudin, K. N.; Staroverov, V. N.; Kobayashi, R.; Normand, J.; Raghavachari, K.; Rendell, A.; Burant, J. C.; Iyengar, S. S.; Tomasi, J.; Cossi, M.; Rega, N.; Millam, J. M.; Klene, M.; Knox, J. E.; Cross, J. B.; Bakken, V.; Adamo, C.; Jaramillo, J.; Gomperts, R.; Stratmann, R. E.; Yazyev, O.; Austin, A. J.; Cammi, R.; Pomelli, C.; Ochterski, J. W.; Martin, R. L.; Morokuma, K.; Zakrzewski, V. G.; Voth, G. A.; Salvador, P.; Dannenberg, J. J.; Dapprich, S.; Daniels, A. D.; Farkas, O.; Foresman, J. B.; Ortiz, J. V.; Cioslowski, J.; Fox, D. J. *Gaussian 09*, revision A.1; Gaussian, Inc.: Wallingford, CT, 2009.

(73) Becke, A. D. Density-functional exchange-energy approximation with correct asymptotic behavior. *Phys. Rev. A* **1988**, *38*, 3098−3100.

(74) Lee, C.; Yang, W.; Parr, R. G. Development of the Colle-Salvetti correlation-energy formula into a functional of the electron density. *Phys. Rev. B* **1988**, *37*, 785−789.

(75) Cossi, M.; Barone, V.; Cammi, R.; Tomasi, J. Ab Initio Study of Solvated Molecules: A New Implementation of the Polarizable Continuum Model. *Chem. Phys. Lett.* **1996**, *255*, 327−335.